

High-Performance and Low-Cost Sodium-Ion Anode Based on a Facile Black Phosphorus-Carbon Nanocomposite

Peng, Bo; Xu, Yaolin; Liu, Kai; Wang, Xiaoqun; Mulder, Fokko M.

DOI

[10.1002/celec.201700345](https://doi.org/10.1002/celec.201700345)

Publication date

2017

Document Version

Accepted author manuscript

Published in

ChemElectroChem

Citation (APA)

Peng, B., Xu, Y., Liu, K., Wang, X., & Mulder, F. M. (2017). High-Performance and Low-Cost Sodium-Ion Anode Based on a Facile Black Phosphorus-Carbon Nanocomposite. *ChemElectroChem*, 4(9), 2140–2144 . <https://doi.org/10.1002/celec.201700345>

Important note

To cite this publication, please use the final published version (if applicable). Please check the document version above.

Copyright

Other than for strictly personal use, it is not permitted to download, forward or distribute the text or part of it, without the consent of the author(s) and/or copyright holder(s), unless the work is under an open content license such as Creative Commons.

Takedown policy

Please contact us and provide details if you believe this document breaches copyrights. We will remove access to the work immediately and investigate your claim.

A High Performance and Low Cost Sodium Ion Anode Based on a Facile Black Phosphorus – Carbon Nanocomposite

Bo Peng,^{†[a,b]} Yaolin Xu,^{†[b]} Kai Liu,^[a] Xiaoqun Wang^[c,a] and Fokko M. Mulder^{*[b]}

Abstract: Black phosphorus (BP) has received increasing research attention as an anode material in sodium ion batteries (SIBs) due to its high capacity, electronic conductivity and chemical stability. However, it is still challenging for BP based SIB anodes to achieve a high electrochemical performance utilizing cost-effective materials and synthetic methods. This work presents a sodium ion anode based on a facile BP – carbon nanocomposite synthesized from commercial red phosphorus and low-cost super P carbon black. Intimate interactions between BP and carbon are present which help to maintain the electrical conduction during cycling and therefore a high cycling stability is achieved. It exhibits a high capacity retention of 1381 mAh g⁻¹ for sodium ion storage after 100 cycles, maintaining 90.5 % of the initial reversible capacity. Such high performance / materials cost ratio may provide direction for future phosphorus based anodes in high energy density SIBs.

Cost-effective and high energy density batteries and battery materials are required to meet the demand of electricity storage. Sodium ion batteries (SIBs) attract increasing research attention because of the high abundance of sodium compared to lithium, and significant progress has been made in recent years.^[1-3] Among the high-capacity anode materials (Sb, Sn, etc.) for sodium ion storage, phosphorus exhibits the highest theoretical capacity of 2596 mAh g⁻¹ (Na₃P). Significant research interest has been triggered by the prospects of high energy density SIBs based on phosphorus anodes.^[4,5]

Phosphorus exists in several allotropes that exhibit strikingly different properties. White phosphorus is chemically unstable, volatile, toxic and non-conducting, and therefore not suitable for battery applications. The most common allotrope, red phosphorus, is widely available and chemically stable, and has been studied intensively for sodium ion batteries.^[6-13] However, its low electrical conductivity appears to be a major drawback. To address this issue, these electrodes included a large amount of costly carbon nanomaterials (graphene, carbon nanotube (CNT), carbon nanofiber (CNF), etc.). For large scale applications the use of CNT's needs orders of magnitude reduced cost levels,^[14] while also graphene and its processing

are considered costly.^[15] With respect to energy density and manufacturing cost these material factors^[16] form a barrier for the commercial introduction of phosphorus as the anode materials for SIBs. Cost-effective super P carbon black are also investigated,^[17] but the cycle life of the electrode (only 30 de-/sodiation cycles were reported) is still to be improved.

The use of carbon should be noted because carbon and phosphorus do not form binary inorganic or molecular compounds; they can, however, form composites of phosphorus and carbon nanostructures held together by what will likely be weak van der Waals forces. The fact that no P-C compounds are stable implies that upon Na insertion and extraction there are no strong P-C bonds to break or there need not be P or C interdiffusion and/or (de-)mixing during the reactions.

It also should be noticed, during the manufacturing of these red phosphorus based SIBs, mechanical ball milling was frequently applied to promote the integration of the conductive carbon matrix as well as to reduce the particle size of the active materials.^[11,12] The presence of black phosphorus was not reported, however, though it can be speculated that red phosphorus might have been partially converted into black phosphorus during ball milling.

Black phosphorus, which appears with a layered structure similar to graphite, is thermodynamically the most stable among the allotropes. Meanwhile, it has a relatively high bulk electronic conductivity (~100 S m⁻¹) and low band gap (0.34 eV). Therefore, it has recently drawn much research attention in various energy storage applications including SIBs.^[18-20] The first black phosphorus–carbon composite was prepared by Ramireddy *et al.* through a ball milling approach from red phosphorus, and the as-synthesized phosphorus-graphite composite achieved a considerable initial capacity (1427 mAh g⁻¹) for SIBs but poor cycling stability (119 mAh g⁻¹ for the 50th cycle).^[21] Since then progress has been made to improve the cycling stability of black phosphorus in SIBs. Cui's group presented a phosphorene (single layer black phosphorus) - graphene hybrid electrode with a reversible sodiation capacity of 2080 mAh g⁻¹ in 100 cycles with respect to the mass of phosphorene present.^[22] Amine's group developed a black phosphorus – Ketjenblack multiwall carbon nanotube composite that exhibits a high specific capacity with excellent cyclability (~1700 mAh g⁻¹ in 100 cycles).^[23] However, these electrodes utilized highly expensive black phosphorus crystals (synthesized under extremely high pressure and temperature^[24]) as the starting materials together with a large amount of costly carbon nanomaterials, including CNT and graphene, as well as sophisticated sample processing. Such costly processing and nanomaterials use will limit the commercial viability of phosphorus based anodes in SIBs as described above.

In this work, black phosphorus and a nanocomposite of the black phosphorus and super P carbon black are facilely synthesized through mechanical ball milling. Such technique can in principle be made continuous and scalable.^[25] Evidence of bonds between phosphorus and carbon can be found, indicating the intimate contacts between black phosphorus and carbon, which may help to maintain the electronic conduction

[a] Bo Peng, Dr. Kai Liu, prof. dr. Xiaoqun Wang
Department of Physics, Renmin University of China
No. 59 Zhongguancun Street, Haidian District, 100872, Beijing, China

[b] Bo Peng, Yaolin Xu, prof. dr. Fokko M. Mulder
Materials for Energy Conversion and Storage (MECS), Department of Chemical Engineering, Faculty of Applied Sciences, Delft University of Technology
Van der Maasweg 9, 2629 HZ Delft, The Netherlands
E-mail: F.M.Mulder@tudelft.nl

[c] prof. dr. Xiaoqun Wang
Department of Physics and Astronomy, Shanghai Jiao Tong University
No. 800 Dongchuan Road, Minhang District, 200240, Shanghai, China

† These authors contributed equally to the work.

Supporting information for this article is given via a link at the end of the document.

during cycling and thus to achieve a high cycling stability in SIBs. The black phosphorus exhibits an initial reversible capacity of 1525 mAh g^{-1} for sodium ion storage and 90.5 % of that can still be retained after 100 cycles, which indicates a significant improvement compared to ref. [21] and a superior performance/cost ratio than previous reports on black phosphorus based SIB anodes.

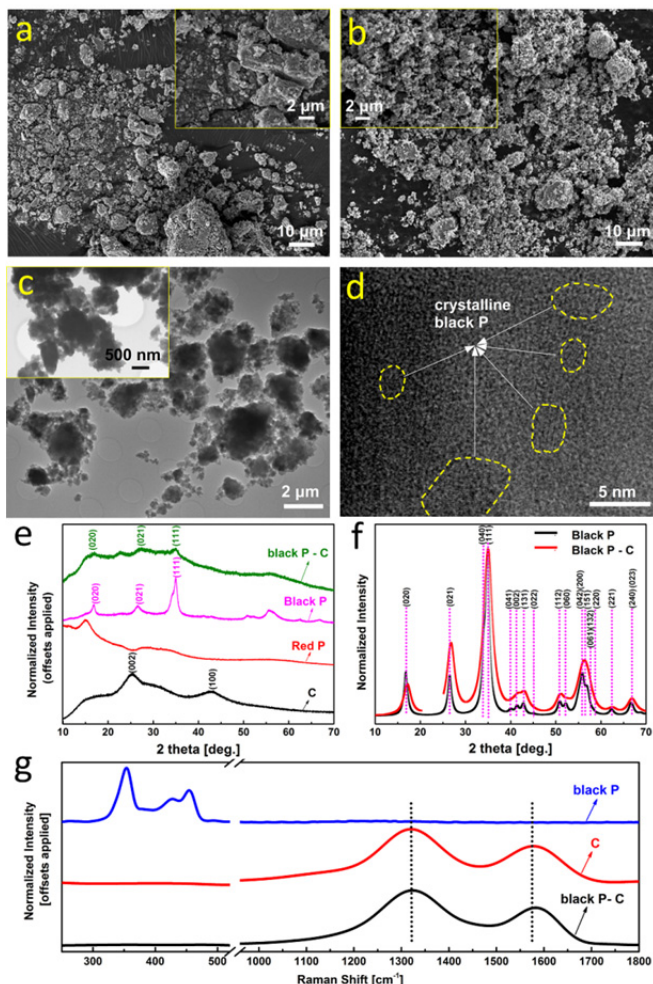


Figure 1. Characterization on the BP-C related samples. (a), SEM images of ball-milled black phosphorus; (b), SEM images of the BP-C composite. (c) – (d), TEM images of the BP-C composite at different magnifications. (e), XRD patterns of super P carbon black, pristine red phosphorus, black phosphorus and the BP-C composite, respectively. (f), Refined XRD patterns of the black phosphorus and the BP-C composite after subtraction of background; (space group: cmce, $a = 3.364$, $b = 10.472$, $c = 4.326$; detailed refinement in **Figure S2**) (g), Raman spectra of super P carbon black, black phosphorus and the as-synthesized BP-C composite.

Black phosphorus (BP) was produced via high energy ball milling from commercial red phosphorus for 70 hours and the BP - carbon composite (BP-C) was prepared by mechanically milling the as-synthesized BP and super P carbon black for 20 hours. (details in **Experimental Section**)

Scanning electron microscope (SEM) images (**Figure 1a**) show that the as-synthesized BP appears as agglomerates of micron and sub-micron scale due to the high energy ball milling. Upon milling with carbon, the BP-C composite appears more

refined (**Figure 1b**). Transmission electron microscope (TEM) images (**Figure 1c & 1d** and **Figure S1** in the **Supporting Information (SI)**) of the BP-C composite shows that the sample is poorly crystalline with, judging from the lattice spacing, nano-domains of crystalline phosphorus embedded in the amorphous carbon matrix. Meanwhile, EDX (Energy-dispersive X-ray Spectroscopy) analysis based on SEM and STEM element mapping (**Figure S2** in the SI) shows that both phosphorus and carbon distribute homogeneously throughout the composite; and oxygen appears on the surface of phosphorus and in the carbon network.

X-ray diffraction (XRD) patterns (**Figure 1e**) reveal that, unlike red phosphorus which is amorphous, black phosphorus shows characteristic crystalline peaks indicating the lattice planes of (020) at 16.8° , (021) at 26.6° and (111) at 35.0° . The grain size of black phosphorus is also gradually reduced for longer durations of ball milling. The average crystalline domain size of black phosphorus reached 8.5 nm using Scherrer's equation and the Rietveld refinement (**Figure 1f** and **Figure S4a** in the SI).

Poorly crystalline Super P carbon black shows two extremely broad characteristic peaks at $2\theta = 25.3^\circ$ and 42.8° corresponding to the Bragg reflection on the (002) and (100) lattice planes. After milling with carbon the BP still shows the characteristic crystalline peaks but they are broader due to the further reduced average crystalline domain size (4.0 nm from the Rietveld refinement in **Figure S4b** in the SI) and thus poor crystallinity, which is also in line with the TEM analysis. We interpret that as a further refinement of BP domain sizes enabled by a separation or refinement due to the presence of carbon that interferes with the aggregation of BP into larger domains. Moreover, apart from the diffraction peaks of BP, a distinct peak at 22.7° appears, which can be attributed to the reflection of the (002) planes of carbon with an increased lattice spacing. Such expansion may be explained by a concentration of phosphorus introduced in the carbon when comparing with XRD patterns of phosphorus doped carbon in literature.^[26,27]

Raman spectra (**Figure 1g**) show the fingerprint Raman bands of black phosphorus corresponding to the A_{1g}, B_{2g} and A_{2g} modes appear at about 354 , 428 , and 454 cm^{-1} , respectively, which vanished after the milling with carbon. This probably results from the encapsulation of carbon on BP and the high optical absorption of the laser in carbon. The Raman spectrum of super P carbon exhibits both the characteristic carbon D (1360 cm^{-1}) and G band (1579 cm^{-1}) of carbon. The G band is related to the first-order scattering of the E_{2g} mode for sp^2 carbon; and the D band is related to structural defects. After ball milling with black phosphorus, a red-shift of the G band by 13 cm^{-1} from 1579 to 1592 cm^{-1} was accrued, which could be attributed to the Van der Waals interactions between BP and carbon and the formation of P-C bond.

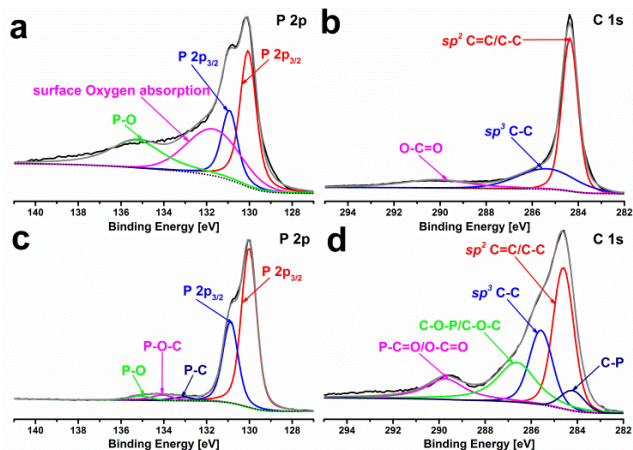


Figure 2. XPS spectra of the samples. (a), P 2p spectrum of black phosphorus; (b), C 1s spectrum of super P carbon black; (c), P 2p, and (d), C 1s of the BP-C composite.

In order to further investigate the interaction between BP and carbon, X-ray photoelectron spectroscopy (XPS) was applied to analyse the surface chemical compositions of the samples (**Figure 2**). Since the samples are treated in air and water when producing the electrodes the materials studied by XPS were also exposed to air before the measurement. In **Figure 2a**, distinct P 2p_{1/2} and P 2p_{3/2} peaks are identified at 130.1 eV and 131.0 eV, respectively. Broad peaks at a higher energy range are also observed, which corresponds to the surface chemisorption of oxygen (131.9 eV) and oxidation of phosphorus (135.4 eV). The C 1s spectrum (**Figure 2b**) illustrates a dominant sp² C=C/C-C (284.4 eV) peak indicating a high graphitization level in the sample; a sp³ carbon peak at 285.4 eV and a low C=O peak at 289.9 eV also appear.

Comparing the XPS spectra of high-energy ball milled BP and the BP-C composite, the characteristic P 2p peak appears to be much more resolved in the latter (**Figure 2c**). It indicates that less oxygen/oxidation exists in black phosphorus which is indicative of encapsulation and thus protection by the carbon network when exposed to air. Meanwhile, indistinctive but observable peaks are attributed to P-C (133.1 eV)^[28-30], P-O-C (134.1 eV)^[30-32] and P-O (135.1 eV)^[29,31]. The presence of chemical bonds between BP and carbon are also evidenced in the C 1s spectrum (**Figure 2d**). Specifically, a C-P bond attributed to phosphorus which is located as doping in the carbon (consistent with the increased carbon lattice spacing from XRD) is located at 284.1 eV; the peak from C-O-P/C-O-C lies at 286.7 eV; and a distinct peak appears at 289.7 eV that can be assigned to P-C=O/O-C=O.^[13,32,33] The bonds with oxygen originate from the oxidation of ball milled carbon upon exposure to air. The BP in the composite shows a marked reduction of the P-O signal. In addition, a more evident appearance C-O/C=O than P-O in the BP-C composite, as well as the higher intensity of the phosphorus - carbon interactions in the C 1s spectrum than in the P 2p range are present. These findings suggest a morphology of black phosphorus encapsulated by carbon rather than an independent uniform distribution of carbon next to phosphorus; oxygen is now seized by the carbon outer layer. This is consistent with the TEM observations that nanosized crystalline phosphorus particles are embedded in the amorphous carbon matrix and the more

concentrated oxygen presence in the carbon network and on the surface of phosphorus particles. Such result indicates a reduced oxidation sensitivity of BP in air in the composite, thus facilitating the low-cost, environmentally-friendly, water based slurry method for electrode production.

With respect to the peaks of carbon, super P carbon black is dominated by sp² carbon. The BP-C composite still contains both sp² and sp³ carbon, but the intensity of the sp² carbon signal is lower, possibly due to a lower level of graphitization in the sample due to the high-energy ball milling.

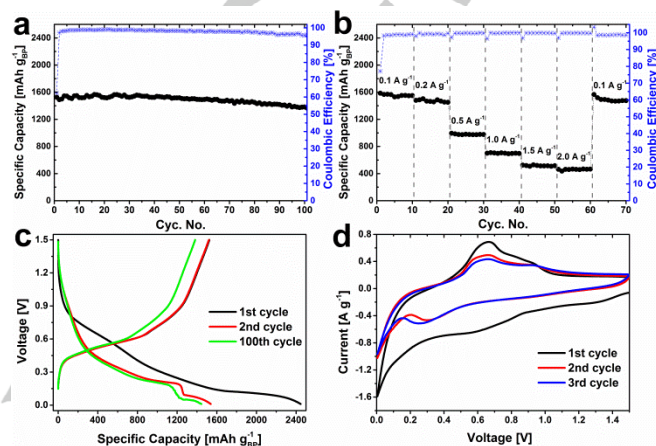


Figure 3. Electrochemical performance of the BP-C composite anode for sodium ion batteries. (a), Capacity retention and Coulombic efficiency cycling at 0.1 A g⁻¹; (b), Rate capability; (c), Voltage profile of the electrode cycling at 0.1 A g⁻¹; (d), Cyclic voltammetry of the electrode for the first 3 cycles. (scan rate: 0.2 mV s⁻¹)

The electrochemical performance of the BP-C composite anode (**Figure 3**) was evaluated within half-cell SIBs. The working electrodes were prepared with a conventional slurry based method using the BP-C composite, super P carbon black and NaCMC with a mass ratio of 8 : 1 : 1 and deionized water as the solvent. The capacity contribution from super P carbon black has been determined in past work^[34] and then subtracted from the BP-C electrode. The specific capacities reported in this paper were the capacity calculated based on the mass of black phosphorus (subtracting of the capacity stored in carbon; the capacity based on the mass of the full BP-C composite is displayed **Figure S5** in the SI). **Figure 3a** shows that, cycling at 0.1 A g⁻¹, the BP-C anode achieved a reversible capacity of 1525 mAh g⁻¹ for sodium ion insertion in the 1st cycle; and the Coulombic efficiency amounts to 62.4 %. The capacity loss in the 1st cycle can be ascribed to irreversible decomposition of electrolyte and solid electrolyte interphase (SEI) formation. The Coulombic efficiency increased to 97.2 % for the 2nd cycle and remained stable close to 100% after that, indicating that the SEI layer is mostly formed during the 1st cycle. Further SEI formation in the following cycles was limited, possibly aided by the use of FEC in the electrolyte.^[35,36] A high capacity of 1381 mAh g⁻¹ was retained after 100 cycles which accounts for 90.5 % of the capacity from the first cycle.

The Rate capability of the electrode (**Figure 3b**) has been studied at various current rates from 0.1 to 2.0 A g⁻¹. The capacities reached 1460, 975, 700 and 465 mAh g⁻¹ at 0.2, 0.5, 1.0 and 2.0 A g⁻¹, respectively. Afterwards a capacity of about

1490 mAh g⁻¹ was obtained when the rate was reset to 0.1 A g⁻¹. These high rate capabilities indicate that the electrical conductivity has been greatly enhanced throughout the electrode by the conducting carbon network that enables good electronic charge transport.

A sloped voltage plateau at ~ 0.6 V originating from the irreversible SEI formation is observed in the 1st sodium ion insertion of the BP-C electrode (Figure 3c); it disappears in the following cycles. This is consistent with the anodic cyclic voltammetry (CV) profiles (Figure 3d). The major sodium ion uptake and formation of Na_xP occurs between 0.5 – 0.2 V vs. Na/Na⁺; while the release of sodium ion mostly takes place between 0.4 – 0.9 V. This is also in accordance with the CV profile. The cathodic peaks at around 0.59 V, 0.69 V and 0.93 V are related to the stepwise release of sodium ion from the fully sodiated phases (Na_xP).

The improved cycling stability in the BP-C electrode when compared to a black phosphorus electrode without carbon addition (rapid capacity degradation over cycling, Figure S6 in the SI), may thus result from the following: (1) As described in the XRD analysis black phosphorus has been downsized to only a few nm through the apparent refinement induced by the presence of carbon. Such further nanoscaling will enable a more rapid kinetics for sodium ion uptake. Moreover, the small grain size may also allow for a higher stress tolerance upon the volume changes that occur during dis-/charge and minimize further particle pulverization as the particles are already small. (2) Interactions between black phosphorus and carbon are present in the sample as deduced from the XRD, Raman and XPS spectra. These interactions help to maintain electrical contact between BP and the carbon network and also preserve the structural integrity of the electrode during cycling.

The improvement in cycling performance compared to ref. [21] will be the beneficial effects of several factors: (1), reduced size of carbon materials which enables better electrical conduction in the composite and more interactions with phosphorus; (2), higher energy applied in the ball milling procedure, which reduces the particle size allowing for faster kinetics and stronger interactions between phosphorus and carbon; (3), increased FEC concentration in the electrolyte which creates a more stable SEI layer and (4), limited voltage window for cycling resulting in ameliorated structural deformation along cycling^[21,37,38].

In summary, we developed a cost-effective, high-performance anode for SIBs based on a facilely synthesized black phosphorus – carbon composite. The active material for the electrode was synthesized via a scalable ball-milling approach utilizing low-cost commercial red phosphorus and super P carbon black starting materials. The synthetic black phosphorus becomes intimately bound within the protective and conducting carbon matrix and a high capacity retention and cycling stability for sodium ion storage has been achieved (1381 mAh g⁻¹ in 100 cycles accounting for 90.5 % of the initial reversible capacity). Taking into account the low cost materials together with the industrially scalable synthesizing approach and compared to the previous studies on black phosphorus based SIB anodes, the facile black phosphorus – carbon composite reported in this work may be considered to exhibits a remarkable performance/cost ratio and may have considerable potential for its commercial introduction in high energy density SIBs.

Experimental Section

Sample synthesis: To synthesize black phosphorus (BP), commercial red phosphorus (Alfa Aesar, 99 %) was mechanically milled for 70 hours at a rotation speed of 400 rpm with a 100:1 ball-to-material mass ratio under 1 bar argon using a Fritsch Planetary Mono Mill PULVERISETTE 6. The BP - carbon composite (BP-C) was prepared by mechanically milling the as-synthesized BP and super P carbon black (TIMCAL) with a mass ratio 7 : 3 for 20 hours at the same milling conditions as used for the BP synthesis.

Characterization: SEM images and the SEM-EDX analysis of the ball-milled samples were taken with a JEOL JSM 6010F scanning electron microscope that operates at an accelerating voltage of 5 kV. TEM images and the STEM-EDX analysis were obtained using a monochromated FEI-Tecnaï with a FEG source at an accelerating voltage of 200 kV. XRD patterns were obtained with a PANalytical X'Pert Pro PW3040/60 diffractometer using a Cu K_α source. The operating voltage and current were 45 kV and 40 mA, respectively. Raman spectroscopy was conducted with a Thermo Scientific Nicolet Almega XR Dispersive Raman Spectrometer. XPS measurement was performed with a K-alpha Thermo Fisher Scientific spectrometer using a monochromatic Al K_α source, and the spectra were analyzed with a Thermo Avantage software.

Electrode preparation: The working electrodes were prepared with a conventional slurry based method using the BP-C composite, super P carbon black and sodium carboxymethyl cellulose (NaCMC) with a mass ratio of 8 : 1 : 1 and deionized water as the solvent. Firstly, the slurry was casted on a Cu foil current collector (12.5 μm, Goodfellow) by doctor blading, followed by drying in a vacuum oven at 70 °C and mechanical compaction with a roller compressor for a good electrical contact. Then it was cut into circular test electrodes with a diameter of 12.7 mm. The mass loading of active materials amounts to ~ 1 mg cm⁻².

Electrochemistry: The electrochemical performance of the BP-C composite based electrodes was evaluated within half-cell SIBs in which sodium metal was used as the counter electrode. A borosilicate glass micro fiber (Whatman) was employed as the separator. 1 M sodium perchlorate (NaClO₄) dissolved in ethylene carbonate (EC) and propylene carbonate (PC) (EC : PC = 1 : 1 in volume) with 10 % fluoroethylene carbonate (FEC) was employed as the electrolyte. Galvanostatic electrochemical performance of the BP-C anode was studied at room temperature using a MACCOR 4600 battery cycler. Cyclic voltammetry (CV) tests were carried out with a PGSTAT302N Autolab potentiostat. The cut-off voltages were 0.005 V and 1.5 V vs. Na/Na⁺ for discharge and charge, respectively.

Acknowledgements

This work is financially supported by the Chinese Scholarship Council (CSC) and the "A green Deal in Energy Materials" (ADEM) grant funded by Dutch Ministry of Economic Affairs and ADEM industrial partners.

Keywords: Black Phosphorus • Nanocomposite • Sodium ion Batteries

- [1] B. L. Ellis, L. F. Nazar, *Curr. Opin. Solid State Mater. Sci.* **2012**, *16*, 168.
- [2] W. Luo, F. Shen, C. Bommier, H. Zhu, X. Ji, L. Hu, *Acc. Chem. Res.* **2016**, *49*, 231.
- [3] H. Kim, H. Kim, Z. Ding, M.H. Lee, K. Lim, G. Yoon, K. Kang, *Adv. Energy Mater.* **2016**, *6*, 1600943.
- [4] M. Dahbi, N. Yabuuchi, K. Kubota, K. Tokiwa, S. Komaba, *Phys. Chem. Chem. Phys.* **2014**, *16*, 15007.

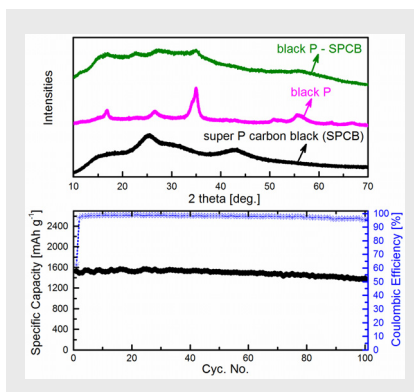
- [5] M. Shimizu, H. Usui, K. Yamane, T. Sakata, T. Nokami, T. Itoh, H. Sakaguchi, *Int. J. Electrochem. Sci.* **2015**, *10*, 10132.
- [6] W. Li, S. H. Hu, X. Luo, Z. Li, X. Sun, M. Li, F. Liu, Y. Yu, *Adv. Mater.* **2017**, *1605820*.
- [7] C. Zhang, X. Wang, Q. Liang, X. Liu, Q. Weng, J. Liu, Y. Yang, Z. Dai, K. Ding, Y. Bando, J. Tang, D. Golberg, *Nano Lett.* **2016**, *16*, 2054-2060.
- [8] W. Li, Z. Yang, M. Li, Y. Jiang, X. Wei, X. Zhong, L. Gu, Y. Yu, *Nano Lett.* **2016**, *16*, 1546.
- [9] W. J. Li, S. L. Chou, J. Z. Wang, H. K. Liu, S. X. Dou, *Nano Lett.* **2013**, *13*, 5480.
- [10] L. Pei, Q. Zhao, C. Chen, J. Liang, J. Chen, *ChemElectroChem* **2015**, *2*, 1652.
- [11] J. Song, Z. Yu, M. L. Gordin, S. Hu, R. Yi, D. Tang, T. Walter, M. Regula, D. Choi, X. Li, A. Manivannan, D. Wang, *Nano Lett.* **2014**, *14*, 6329.
- [12] J. Song, Z. Yu, M. L. Gordin, X. Li, H. Peng, D. Wang, *ACS Nano* **2015**, *9*, 11933.
- [13] B. Ruan, J. Wang, D. Shi, Y. Xu, S. Chou, H. Liu, J. Wang, *J. Mater. Chem. A* **2015**, *3*, 19011.
- [14] M.F.L. De Volder, S.H. Tawfick, R.H. Baughman, A.J. Hart, *Science* **2013**, *339*, 535-539.
- [15] K. S. Novoselov, V.I. Falko, L. Colombo, P.R. Gellert, M.G. Schwab, K. Kim, *Nature* **2012**, *490*, 192-200.
- [16] Y. Gogotsi, P. Simon, *Science* **2011**, *334*, 917-918.
- [17] Y. Kim, Y. Park, A. Choi, N.-S. Choi, J. Kim, J. Lee, J. H. Ryu, S. M. Oh, K. T. Lee, *Adv. Mater.* **2013**, *25*, 3045.
- [18] K. P. S. S. Hembram, H. Jung, B. C. Yeo, S. J. Pai, S. Kim, K. R. Lee, S. S. Han, *J. Phys. Chem. C* **2015**, *119*, 15041.
- [19] V. V. Kulish, O. I. Malyi, C. Persson, P. Wu, *Phys. Chem. Chem. Phys.* **2015**, *17*, 13921-13928.
- [20] L. Q. Sun, M. J. Li, K. Sun, S. H. Yu, R. S. Wang, H. M. Xie, *J. Phys. Chem. C* **2012**, *116*, 14772.
- [21] J. Sun, H.-W. Lee, M. Pasta, H. Yuan, G. Zheng, Y. Sun, Y. Li, Y. Cui, *Nat. Nanotechnol.* **2015**, *10*, 980.
- [22] G. L. Xu, Z. Chen, G. M. Zhong, Y. Liu, Y. Yang, T. Ma, Y. Ren, X. Zuo, X. H. Wu, X. Zhang, K. Amine, *Nano Lett.* **2016**, *16*, 3955.
- [23] P. W. Bridgman, *J. Am. Chem. Soc.* **1914**, *36*, 1344.
- [24] T. Ramireddy, T. Xing, M. M. Rahman, Y. Chen, Q. Dutercq, D. Gunzelmann, A. M. Glushenkov, *J. Mater. Chem. A* **2015**, *3*, 5572.
- [25] P. Baláz, in *Mechanochemistry in Nanoscience and Minerals Engineering*, Springer Berlin Heidelberg, **2008**, pp. 103-132.
- [26] J. Wu, Z. Yang, Q. Sun, X. Li, P. Strasser, R. Yang, *Electrochim. Acta* **2014**, *127*, 53-60.
- [27] J. Wu, C. Jin, Z. Yang, J. Tian, R. Yang, *Carbon* **2015**, *82*, 562-571.
- [28] J. Zhu, S.P. Jiang, R. Wang, K. Shi, P.K. Shen, *J. Mater. Chem. A* **2014**, *2*, 15448-15453.
- [29] J.-S. Li, Y. Wang, C.-H. Liu, S.-L. Li, Y.-G. Wang, L.-Z. Dong, Z.-H. Dai, Y.-F. Li, Y.-Q. Lan, *Nat. Commun.* **2016**, *7*, 11204.
- [30] J.M. Rosas, R. Berenguer, M.J. Valero-Romero, J. Rodríguez-Mirasol, T. Cordero, *Front. Mater.* **2014**, *1*, 29.
- [31] W. Qi, H. Zhao, Y. Wu, H. Zeng, T. Tao, C. Chen, C. Kuang, S. Zhou, Y. Huang, *Sci. Rep.* **2017**, *7*, 43582.
- [32] J. Sun, H.-W. Lee, M. Pasta, Y. Sun, W. Liu, Y. Li, H. R. Lee, N. Liu, Y. Cui, *Energy Storage Mater.* **2016**, *4*, 130-136.
- [33] J. Sun, G. Zheng, H.-W. Lee, N. Liu, H. Wang, H. Yao, W. Yang, Y. Cui, *Nano Lett.* **2014**, *14*, 4573;
- [34] Y. Xu, E. Swaans, S. Basak, H. W. Zandbergen, D. M. Borsa, F. M. Mulder, *Adv. Energy Mater.* **2016**, *6*, 1501436.
- [35] M. Dahbi, N. Yabuuchi, M. Fukunishi, K. Kubota, K. Chihara, K. Tokiwa, X.-f. Yu, H. Ushiyama, K. Yamashita, J.-Y. Son, Y.-T. Cui, H. Oji, S. Komaba, *Chem. Mater.* **2016**, *28*, 1625.
- [36] N. Yabuuchi, Y. Matsuura, T. Ishikawa, S. Kuze, J.-Y. Son, Y.-T. Cui, H. Oji, S. Komaba, *ChemElectroChem* **2014**, *1*, 580.
- [37] C.-M. Park, H.-J. Sohn, *Adv. Mater.* **2007**, *19*, 2465-2468.
- [38] B. Mortemard De Boisse, D. Carlier, M. Guignard, L. Bourgeois, C. Delmas, *Inorg. Chem.* **2014**, *53*, 11197-11205.

Entry for the Table of Contents (Please choose one layout)

Layout 1:

COMMUNICATION

A black phosphorus – carbon nanocomposite is facilely synthesized from commercial red phosphorus and low-cost super P carbon black, and it exhibits an excellent performance/cost ratio, remarkable capacity retention and cycling stability as the anode for sodium ion batteries.



Bo Peng, Yaolin Xu, Kai Liu, Xiaoqun Wang and Fokko M. Mulder*

Page No. – Page No.

A High Performance and Low Cost Sodium Ion Anode Based on A Facile Black Phosphorus – Carbon Nanocomposite

1, TEM image of the BP-C composite.

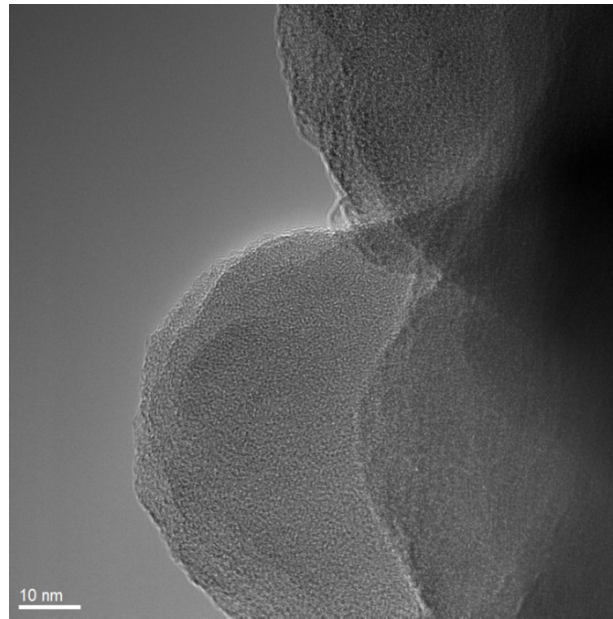


Figure S1. TEM image of the BP-C composite.

2, SEM-EDX characterization on the BP-C composite

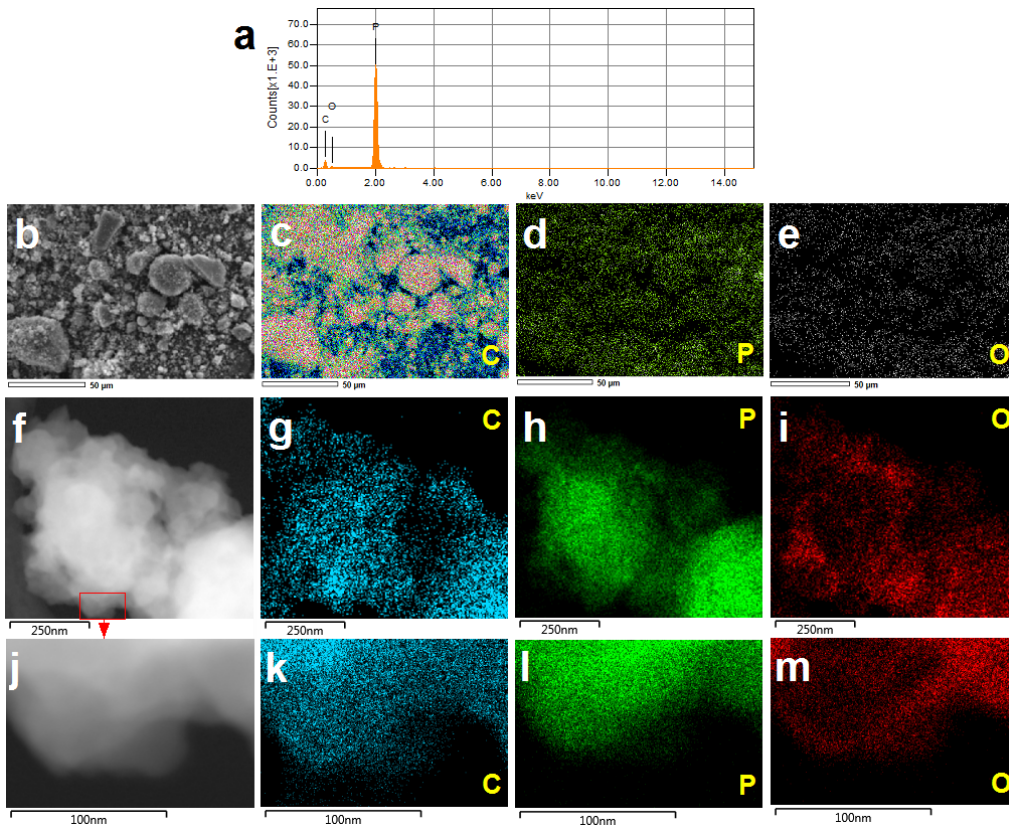


Figure S2: (a), SEM-EDX spectrum and (b) - (e), SEM based EDX element mapping results (scale bar: 50 μm): the layered SEM image and the element mapping of C, P and O in the BP-C composite, respectively. (f) - (m), STEM based EDX mapping results (scale bars: 250 nm and 100 nm, respectively).

3, XRD analysis on the samples

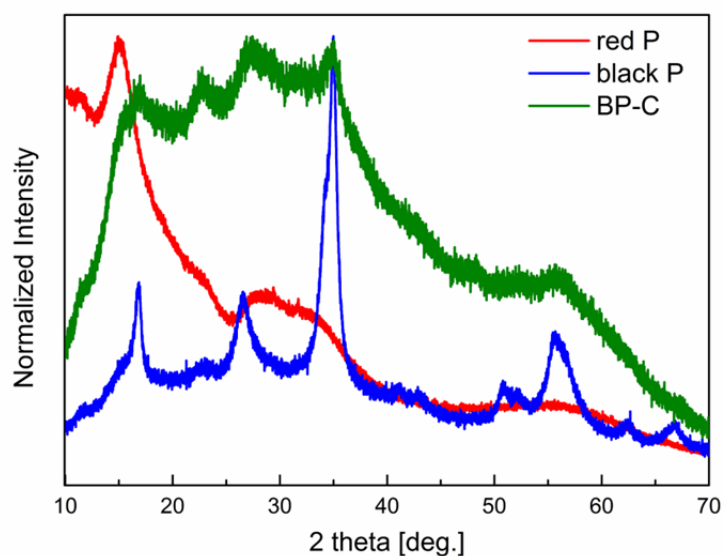


Figure S3. Normalized XRD patterns of the pristine red P, as-synthesized black P and the BP-C composite.

Rietveld refinement on the XRD patterns of black phosphorus and the BP-C composite was carried out within the General Structure Analysis System (GSAS) software suite.[1]

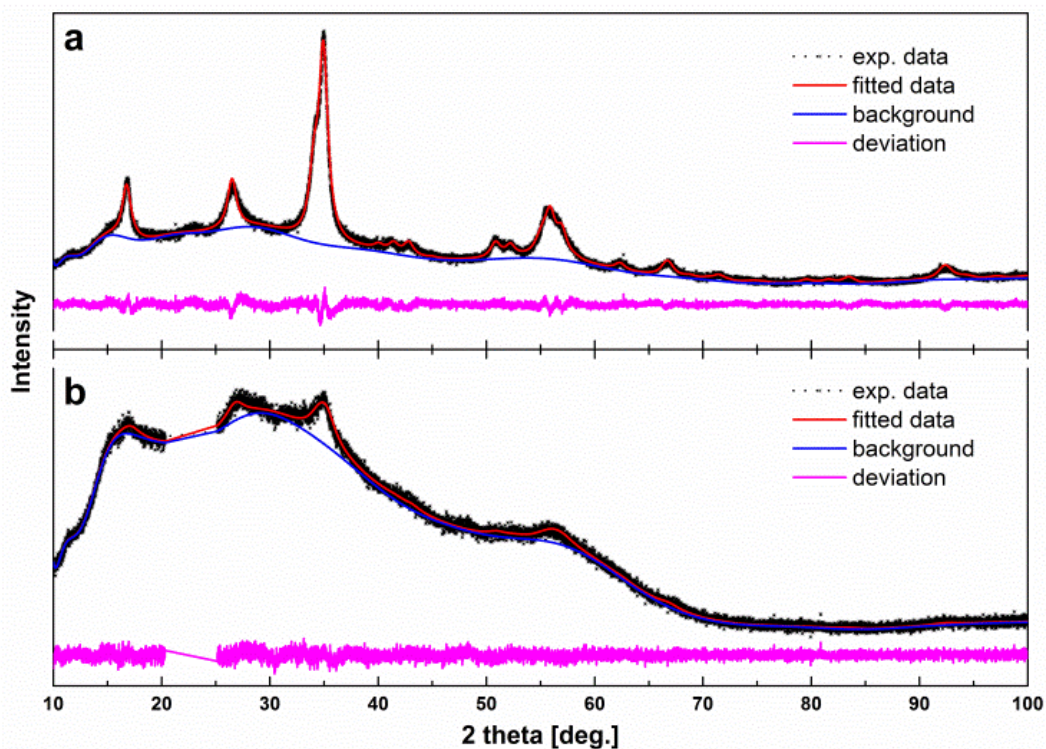


Figure S4. Rietveld Refinement on the black phosphorus (space group: *Cmce*) phase in the XRD patterns of (a), the ball-milled BP and (b), the BP-C composite. (In Figure (b), the 2 theta range of black phosphorus doped carbon was subtracted to achieve an accurate refinement.)

Detailed results on the refinement are displayed in the table below.

samples	Space group	Lattice parameters [Å]	Atom coordinates	U_{iso}	Avg. domain size [nm]
black phosphorus	<i>Cmce</i>	$a = 3.327, b = 10.490, c = 4.352$	8f (0, 0.1018, 0.06772)	0.01785	8.5
BP-C composite	<i>Cmce</i>	$a = 3.364, b = 10.472, c = 4.326$	8f (0, 0.1119, 0.08827)	0.04437	4.0

Table S1: Detailed Rietveld refinement results on the black phosphorus phase in the as-synthesized BP and in the BP-C composite. Note the reduced crystalline domain size and the increased atomic displacement factor U_{iso} in the composite (indicative of somewhat increased disorder in the position of the phosphorus atoms).

4, Electrochemical performance of the BP-C composite based anodes for SIBs

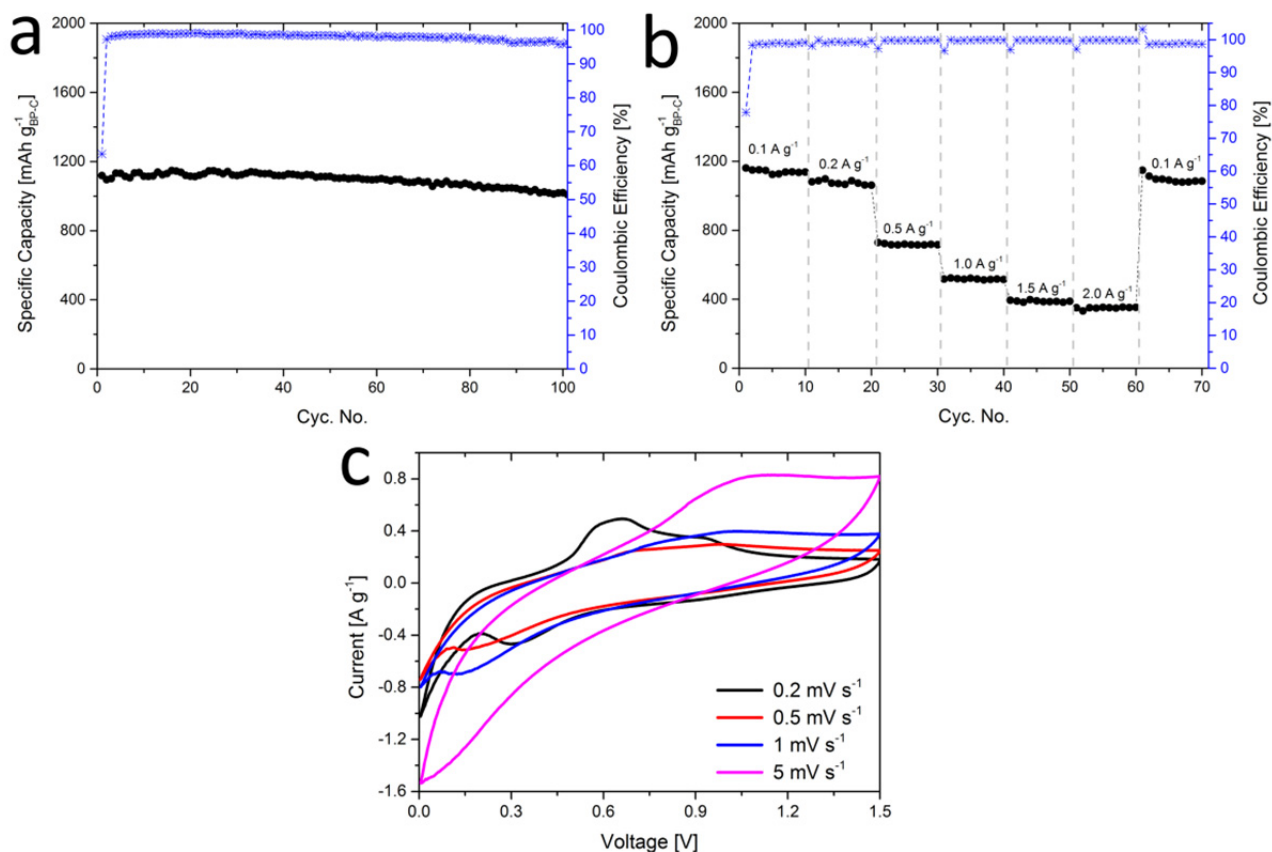


Figure S5. Electrochemical performance. (a), Capacity retention and Coulombic efficiency at 0.1 A g⁻¹ and (b), Rate capability of the BP-C composite based electrodes for sodium ion batteries with respect to the total mass of the BP-C composite. (c), Cyclic voltammetry of the BP-C electrode at different scan rates.

5, A comparison between BP with and without carbon based SIB anodes

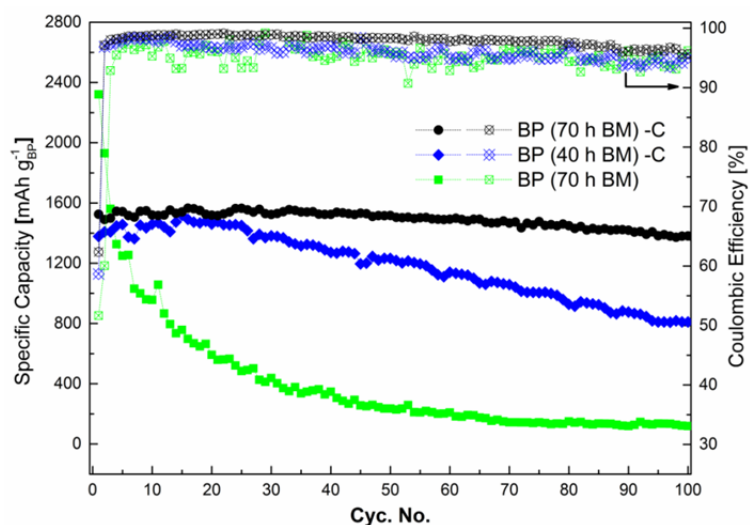


Figure S6. Electrochemical performance of sodium ion anodes based on black phosphorus with and without carbon. (The BP electrode was prepared with the same procedure that was applied in the BP-C electrode fabrication and the dis-/charge rate was 0.1 A g^{-1} .)

6, Micro-morphologies of the phosphorus sample at different stages

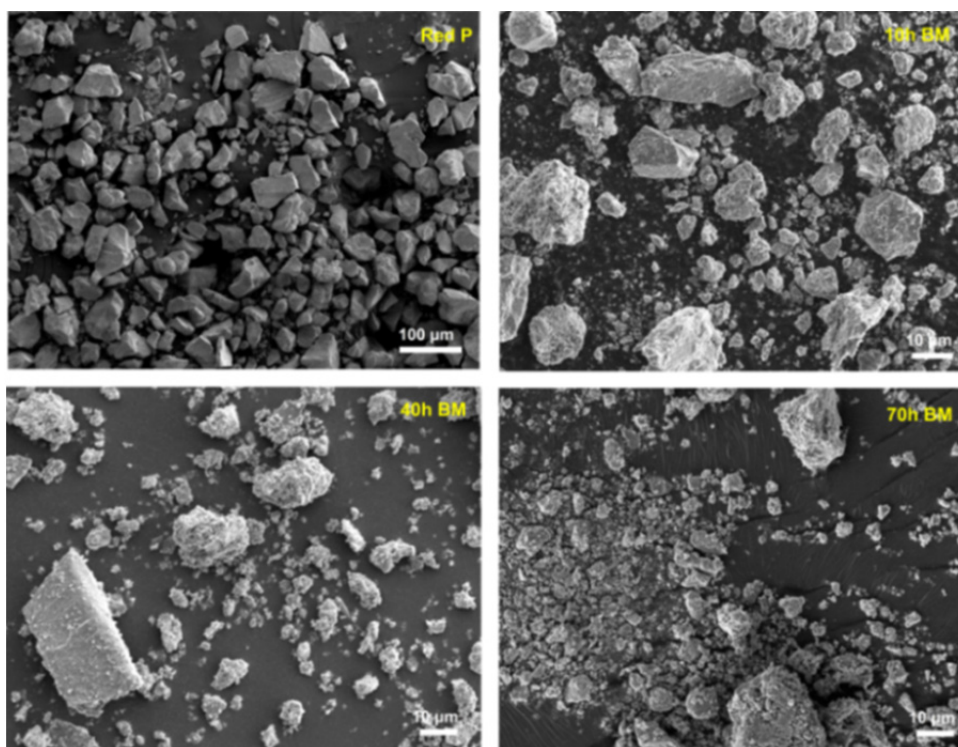


Figure S7. SEM images of phosphorus at different ball-milling stages: (a), pristine red phosphorus; (b), after 10 h milling; (c), after 40 h milling; (d), after 70 h milling.

References:

- [1] A.C. Larson and R.B. Von Dreele, Los Alamos National Laboratory Report LAUR 86-748 (2000).